



## Theoretical and Experimental Inhibitive Properties of Mild Steel in Phosphoric Acid by Clove Essential Oil

L. Adardour<sup>1</sup>, M. Saadouni<sup>2</sup>, Y. El Aoufir<sup>1,3\*</sup>, A. El khlifi<sup>4</sup>, Y. Kerroum<sup>3</sup>, A. Zarrouk<sup>5</sup>,  
A. Guenbour<sup>3</sup>, M. Taleb<sup>6</sup>, S. Boukhriss<sup>2</sup>, H. Oudda<sup>1</sup>

*1. Laboratory of Separation Processes, Faculty of Sciences, University Ibn Tofail, Kenitra, Morocco*

*2. Laboratory of Organic, Organometallic and Theoretical Chemistry, Faculty of Science, Ibn Tofail University, 14000 Kenitra, Morocco*

*3. Laboratory of Nanotechnology, Materials & Environment, Faculty of Sciences, Mohammed V University, Rabat, Morocco*

*4. Laboratoire de Biotechnologie, Environnement et Qualité, Faculté des Sciences, Université Ibn Tofail, 14000 Kénitra*

*5. LCAE-URAC18, Faculté des Sciences, Université Mohammed 1<sup>er</sup>, Oujda, Morocco*

*6. Laboratoire d'Ingénierie de Modélisation et d'Environnement, Faculté des Sciences Dhar El Mehraz FES B.P. 1796 Atlas Fès MAROC.*

Received 01 Aug 2017,  
Revised 26 May 2018,  
Accepted 28 May 2018

### Keywords

- ✓ Mild steel;
- ✓ Phosphoric acid
- ✓ Corrosion inhibition ;
- ✓ Clove oil
- ✓ EIS;
- ✓ PDP

Y. El Aoufir :  
[eyasminal@gmail.com](mailto:eyasminal@gmail.com)

### Abstract

The inhibition performance of clove oil (CLO) on mild steel (MS) in 2 M H<sub>3</sub>PO<sub>4</sub> was studied by weight loss, potentiodynamic polarization and electrochemical impedance spectroscopy (EIS). The adsorption of inhibitor on MS surface obeyed the Langmuir's adsorption isotherm. Potentiodynamic polarization measurements showed that CLO is mixed type. The optimum concentration of 1g/L can decrease the corrosion of material with the efficiency of 87%. The scanning electron microscope (SEM) observations confirmed the existence of a protective film of inhibitor on MS surface. The adsorption behavior of the inhibitor on Fe surface has been studied using molecular dynamics (MD) method and density functional theory. The results indicated that the inhibitor could adsorb on the Fe surface firmly through the benzene ring and two oxygen atoms.

## 1. Introduction

Mild steel is widely used in the fabrication of reaction vessels, storage tanks and petroleum refineries. Corrosion of mild steel is a fundamental academic and industrial concern that has received a considerable amount of attention [1–14]. Furthermore, the corrosion resistance of materials to the phosphoric acid has generally studied in many industrial applications, like in wet process phosphoric acid and pickling Acids [15,16]

Among numerous corrosion prevention measurements, the use of inhibitors is one of the most efficient alternatives to protect metals against corrosion, especially in acidic media due to its advantages of economy, high efficiency, and wide applicability [17–22].

Almost all organic molecules containing hetero atoms such as nitrogen, sulphur, phosphorous and oxygen show significant inhibition efficiency. Despite these promising findings of possible corrosion inhibitors, most of these substances are not only expensive but also toxic non-biodegradable thus causing pollution problems. In view of the disadvantages of the compounds of synthetic origin, there has been a development in the selection of compounds of natural origin for their corrosion inhibition effect. Currently, the research is oriented to the development of "green corrosion inhibitors" with good efficiency and low risk of environmental pollution [23–26]. Oils are sources of naturally occurring compounds, some with complex molecular structures and having different chemical, biological, and physical properties.

This aroused the interest of authors to select the clove oil as a corrosion inhibitor for mild steel in acidic medium. Cloves are the aromatic dried flower buds of a tree *Eugenia caryophyllata* in the family Myrtaceae found in India and other parts of the Far East. Steam distillation of freshly ground cloves results in clove oil

which consists of several compounds. Eugenol (Figure 1) is the main compound comprising 74%. Eugenol acetate comprises 16% [27,28]. Eugenol is a member of the allyl benzene class of chemical compounds. It is a clear to pale yellow oily liquid it is slightly soluble in water and soluble in organic solvents. It has pronounced antiseptic and anaesthetic properties. Eugenol is used in perfumeries, flavorings, essential oils and in medicine as a local antiseptic and anaesthetic [28–30].

Hence, in the present investigation, an attempt has been made to use the clove oil (CLO) for the corrosion inhibition of MS in 2 M H<sub>3</sub>PO<sub>4</sub>. The investigations were made using of electrochemical and weight loss methods. The protective film formed on the metal surface was characterized with the help of SEM analysis. Quantum chemical calculations based on density functional theory (DFT) have been sufficiently developed as a powerful technique to study the interaction between inhibitors and metal surfaces[31,32]. The application of DFT-based calculations in the present case is constructed on the point that several theoretical parameters can be derived for even a complex molecule at a very low cost [33].

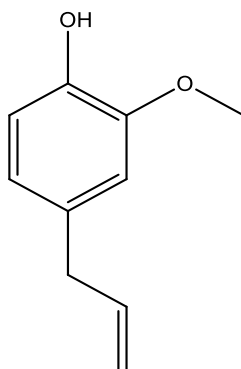


**Figure 1:** Molecular structure of Eugenol.

## 2. Experimental details

### 2.1. Electrodes, chemicals and test solution

Corrosion tests have been performed, using the gravimetric and electrochemical measurements, on electrodes cut from sheets of carbon steel with the chemical composition: 0.370 % C, 0.230 % Si, 0.680 % Mn, 0.016 % S, 0.077 % Cr, 0.011 % Ti, 0.059 % Ni, 0.009 % Co, 0.160 % Cu, and the remainder iron. The aggressive medium of phosphoric acid used for all studies were prepared by dilution of analytical grade 85% H<sub>3</sub>PO<sub>4</sub> with double distilled water. The concentrations of **CLO** (Purchased from the local markets)used in this investigation were varied from 0.25 to 1.00 g/L.

### 2.2. Gravimetric measurements

Gravimetric measurements were realized in a double walled glass cell equipped with a thermostat-cooling condenser. The carbon steel specimens used have a rectangular form with dimension of 2.5×2.0×0.2 cm were abraded with a different grade of emery paper (320-800-1200) and then washed thoroughly with distilled water and acetone. After weighing accurately, the specimens were immersed in beakers which contained 100 ml acid solutions without and with various concentrations of **CLO** at temperature equal to 298 K remained by a water thermostat for 6h as immersion time. The gravimetric tests were performed by triplicate at same conditions. The corrosion rates (*C<sub>R</sub>*) and the inhibition efficiency (*η<sub>wL</sub>* %) of mild steel have been evaluated from mass loss measurement using the following equations:

$$\eta_w = \frac{C_R - C_R^*}{C_R} \times 100 \quad (1)$$

$$\theta = 1 - \frac{C_R^*}{C_R} \Rightarrow \theta = \frac{(\eta_w \%)}{100} \quad (2)$$

Where *C<sub>R</sub>* and *C<sub>R</sub>*<sup>\*</sup> are the corrosion rates of the mild steel in phosphoric acid without and with the studied range of the **CLO** concentrations, respectively, *θ* is the degree of surface coverage.

### 2.3. Electrochemical measurements

Electrochemical measurements, including stationary methods (PDP) and transient (EIS) were performed in a three-electrode cell. The carbon steel specimen was used as the working electrode, saturated calomel (SCE) as reference and area platinum as counter electrode (CE) were used. All potentials were measured against SCE.

The working electrode was immersed in a test solution for 30 min until the corrosion potential of the equilibrium state ( $E_{\text{corr}}$ ) was achieved using a type PGZ100 potentiostat. The potentiodynamic polarization curves were determined by a constant sweep rate of 1 mV/s. The measurements of the transitory method (EIS) were determined, using ac signals of amplitude 10 mV peak to peak at different conditions in the frequency range of 100 kHz to 10 mHz. The data obtained by EIS method were analyzed and fitted using graphing and analyzing impedance software, version *Zview2*. For PDP method, the inhibition efficiency of the studied compound was calculated using the following equation:

$$\eta_{\text{PDP}} (\%) = \left[ 1 - \frac{i_{\text{corr}}}{i_{\text{corr}}^{\circ}} \right] \times 100 \quad (3)$$

where  $i_{\text{corr}}$  and  $i_{\text{corr}}^{\circ}$  are the corrosion rates in the presence and absence of inhibitor, respectively. The impedance diagrams were determined by EIS method. To confirm reproductibility, all experiments were repeated three times and the evaluated inaccuracy does not exceed 10%. For EIS method, the inhibition efficiency was calculated using the following equation:

$$\eta_{\text{EIS}} (\%) = \left[ \frac{R_{\text{p(inh)}} - R_{\text{p}}}{R_{\text{p(inh)}}} \right] \times 100 \quad (4)$$

$R_{\text{p}}$  and  $R_{\text{p(inh)}}$  were the polarisation resistance of mild steel electrode in the uninhibited and inhibited solutions, respectively.

#### 2.4. SEM

The changes of the surface morphology of the mild steel in absence and in presence of the optimum concentration of CLO was studied using Scanning Electron Microscopy (SEM) after 6h of immersion at 303 K. SEM (Hitachi TM-1000) with an accelerating voltage of 15 kV was used for the experiments.

#### 2.5. Computational chemistry calculations

Quantum chemical calculations were carried out using the SPARTAN14 software [34]. The molecular optimization of the Eugenol was achieved using the functional hybrid B3LYP density functional theory (DFT) formalism, having an electron basis set 6-31G (d, p) for all atoms. The molecular dynamics (MD) simulations were performed using the software, Materials Studio [35]. The MD calculation of the simulation of the interaction between Eugenol and the iron surface was carried out in a simulation box ( $24.82 \times 24.82 \times 35.69 \text{ \AA}^3$ ) with periodic boundary conditions to model a representative part of the interface devoid of any arbitrary boundary effects. The box consisted of a Fe slab and a water layer with Eugenol. The Fe crystal was cleaved along the (110) plane with the uppermost and the lowest layers released and the inner layer fixed. The MD simulation was performed under 298 K, NVT ensemble, with a time step of 0.1 fs and simulation time of 10 ps. The interaction energy of the Fe surface with the inhibitor was calculated according to the following equation [36,37]:

$$E_{\text{interaction}} = E_{\text{total}} - (E_{\text{surface+solution}} + E_{\text{inhibitor}})$$

with  $E_{\text{total}}$  being the total energy of the Fe crystal together with the adsorbed inhibitor and water molecules,  $E_{\text{surface+solution}}$  and  $E_{\text{inhibitor}}$  being the total energy of the Fe crystal with water molecules and free inhibitor molecular, respectively. And the binding energy was the negative value of the interaction energy  $E_{\text{Binding}} = -E_{\text{interaction}}$  [38].

### 3. Results and discussion

#### 3.1. Polarization results

The polarization curves for mild steel in the absence and presence of clove oil of different concentrations are shown in Figure 2. The values obtained from polarization curves such as corrosion potential ( $E_{\text{corr}}$ ), corrosion current density ( $i_{\text{corr}}$ ), anodic and cathodic Tafel slopes ( $\beta_a$  and  $\beta_c$ ) were obtained from the intersection of anodic and cathodic Tafel lines, and corrosion inhibition efficiencies  $\eta_{\text{PDP}} (\%)$  were calculated and shown in Table 1.

An inspection of Figure 2 and Table 1 suggests that the presence of clove oil causes a remarkable decrease in the  $i_{\text{corr}}$  values by shifting both the anodic and cathodic Tafel slopes toward low current. Moreover, all the cathodic curves were nearly parallel, suggesting that the mechanism of the cathodic reactions did not change in the presence of the inhibitor and the mechanism of this reaction on inhibited and uninhibited iron in 2 M  $\text{H}_3\text{PO}_4$  is the same [39]. In the anodic range, a fluctuation appears when the potential reaches the -300 mV/SCE. This is

because, at higher anodic potential, the protective properties of adsorbed oil molecules deteriorate and the predominant process is the dissolution of steel [40]. It can also be seen that both the anodic and cathodic currents were shifted to lower values at almost the same potential with the increasing concentration of the inhibitor. This behavior indicates that both the anodic and cathodic reactions were suppressed, i.e., CLO is a mixed-type inhibitor [17,20].

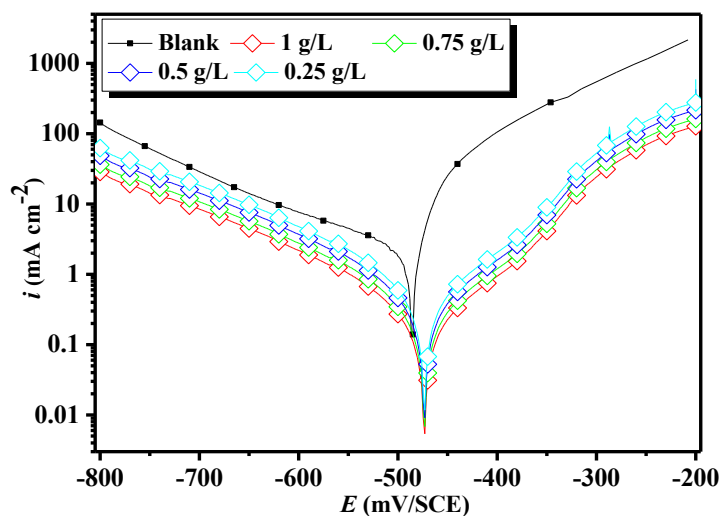


**Figure 2:** Potentiodynamic polarization curves for mild steel in 2 M  $H_3PO_4$  solution in the presence and absence of different concentrations of CLO at 298 K.

**Table 1.** The electrochemical parameters calculated by the PDP technique for the corrosion of mild steel in 2 M  $H_3PO_4$  in the absence and presence of different concentrations of CLO at 298 K.

Inhibitor	Concentration (g/L)	$-E_{corr}$ (mV/SCE)	$-\beta_c$ (mV/dec)	$\beta_a$ (mV/dec)	$i_{corr}$ ( $\mu A/cm^2$ )	$\eta_{PDP}$ (%)
$H_3PO_4$	2 M	488	135	92	2718	-
CLO	0.25	473	179	73	976	64
	0.5	474	177	77	787	71
	0.75	475	181	74	565	79
	1	473	183	71	450	83

### 3.2. Electrochemical impedance spectroscopy (EIS)

The kinetics of the electrode processes and surface properties of the investigated system can be observed by using electrochemical impedance spectroscopy. Figure 3 shows the impedance spectra of mild steel in the form of Nyquist plots for clove oil at different concentration. Figure 3 has a single semicircle at high frequency, which tells the charge transfer of the corrosion process and also the diameter of semicircle of the studied inhibitor increased with the increase of the concentration [10,11,41]. The impedance spectra are not perfect semicircle and it is depressed with center under real axis and resembles depressed capacitive loops. This phenomenon often corresponds to surface heterogeneity, which may be the result of surface roughness, dislocations, distribution of the active sites, or adsorption of the oil molecules [42].

Equivalent circuits are usually used to analyze EIS data [4,8,43]. For example, Figure 4 shows a simple equivalent circuit with one-time constant that is commonly used to analyze the measured impedance of a uniformly corroding electrode in an electrolyte. It consists of an electrolyte resistance ( $R_s$ ), a polarization resistance ( $R_p$ ) and a constant phase element (CPE), which is used for a non-ideal double layer. The impedance of this element is frequency-dependent and can be calculated using the Equation 5:

$$Z_{CPE} = \frac{1}{Q(j\omega)^n} \quad (5)$$

Where  $Q$  is the CPE constant (in  $\Omega^{-1} S^n cm^{-2}$ ),  $\omega$  is the angular frequency (in  $rad s^{-1}$ ),  $j^2 = -1$  is the imaginary number and  $n$  is a CPE exponent which can be used as a gauge for the heterogeneity or roughness of the

surface[44,45]. In addition, the double layer capacitances,  $C_{dl}$ , for a circuit including a  $CPE$  were calculated by using the following Equation 6:

$$C_{dl} = \sqrt[n]{Q \times R_p^{1-n}} \quad (6)$$

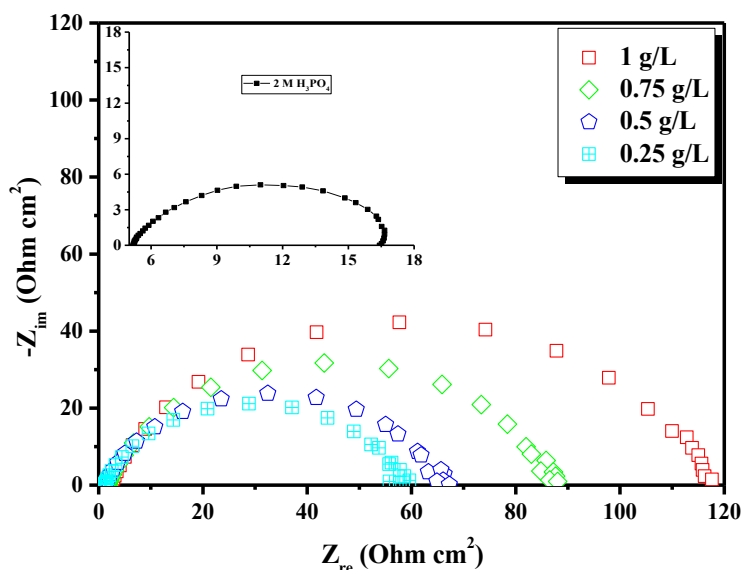


**Fig.3:** Nyquist plots for carbon steel in 2 M  $H_3PO_4$  solution containing various concentrations of CLO at 298 K.

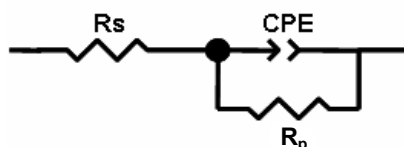


**Figure4:**Equivalent electrical circuit.

The  $\eta_{EIS}$  (%) value is expected to increase as the concentration of the inhibitor is increased, exactly as is found and shown in Table 2. It is also clear from the results depicted in Table 2 that the value of  $R_p$  increases whereas the value of  $C_{dl}$  decreases in the presence of clove oil. This increase in  $R_p$  and decrease in  $C_{dl}$  are attributed due to a decrease in the local dielectric constant and/or to an increase in the thickness of the electrical double layer[46]. It is well known that capacitance is the reciprocal of the thickness of the double layer[47]. A low values of capacitance may also result a larger replacement of water molecules by the almond oil molecules through the adsorption at electrode surface[47]. Also larger molecules of the inhibitor may also reduce the capacitance through an increase in double layer capacitance. Moreover, the thickness of protective layer increased by increasing the inhibitor concentration result a significant decrease in  $C_{dl}$ .

**Table 2.** Impedance parameters recorded for mild steel electrode in 2 M  $H_3PO_4$  solution in the absence and presence of different concentrations of inhibitor at 298K.

Inhibitor	Concentration (g/L)	$R_p$ ( $\Omega \text{ cm}^2$ )	$Q \times 10^{-4}$ ( $s^n \Omega^{-1} \text{ cm}^{-2}$ )	$n$	$C_{dl}$ ( $\mu\text{F/cm}^2$ )	$\eta_{EIS}$ (%)
Blank	2.0	14	2.1024	0.88	94	—
CLO	0.25	56	1.1106	0.85	45	75
	0.5	63	0.9569	0.86	41	77
	0.75	81	0.6994	0.87	32	82
	1	113	0.5115	0.88	25	87

### 3.3. Adsorption isotherm

The adsorption of the inhibitor on the metal surface is the most important topics in corrosion researches because it provides some structural as well as thermodynamic information of the electric double layer [19,20,48]. The adsorption isotherm gives basic information on the interactions between the inhibitor and the steel surface

[49,50]. In our present study several isotherms were tested but Langmuir adsorption isotherm gives the best fit with the values of regression coefficient close to unity. The Langmuir isotherm can be represented as [51]:

$$\frac{C_{\text{inh}}}{\theta} = \frac{1}{K_{\text{ads}}} + C_{\text{inh}} \quad (7)$$

where  $C_{\text{inh}}$  is the concentration,  $K_{\text{ads}}$  is the equilibrium constant of the adsorption process.  $K_{\text{ads}}$  are related to the standard free energy of adsorption  $\Delta G_{\text{ads}}^{\circ}$  by the following equation [51]:

$$\Delta G_{\text{ads}}^{\circ} = -RT \ln(K_{\text{ads}} \times 999) \quad (8)$$

where R represents the gas constant and T is the absolute temperature. The value of 999 is the concentration of water in solution in g/L.

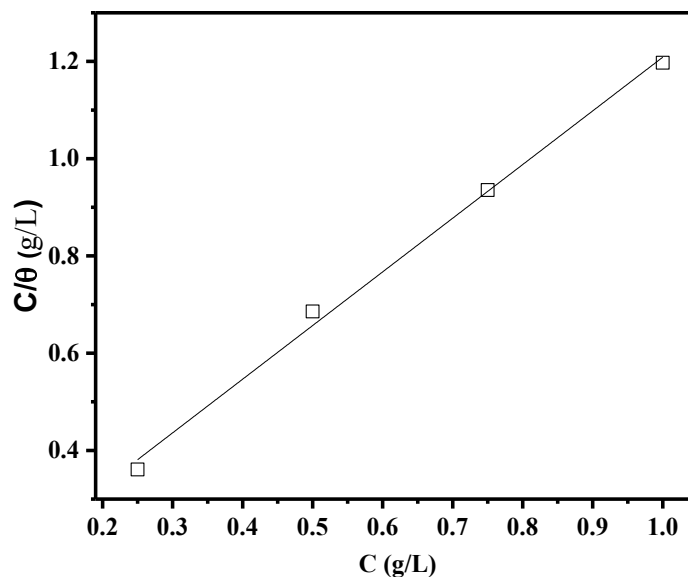


**Figure 5:** Langmuir adsorption of inhibitor on the mild steel surface in 2 M  $\text{H}_3\text{PO}_4$  solution at 298K.

It should be noted that in the case of oils, inhibitory action is related to the intermolecular synergistic effect if the various components [51]. It is safely recommended to not determine  $\Delta G_{\text{ads}}^{\circ}$  values since the mechanism of adsorption remains unknown.

### 3.4. Weight loss study

#### 3.4.1. Effect of concentration

The weight loss parameters such as corrosion rate ( $C_R$ ), surface coverage ( $\theta$ ) and percentage inhibition efficiency ( $\eta_w$  %) are given in Table 3. The weight loss study shows that inhibition efficiency increases with CLO concentration and acquires maximum value of 83% at 1 g/L concentration. We remark that Eugenol provided more inhibition of steel corrosion in molar HCl (91% at 174 g/l) [52]. The highest inhibition efficiency of oil can be attributed due to the presence of  $\pi$ -system and electron releasing  $-\text{OH}$  and  $-\text{OCH}_3$  groups.

**Table 3.** Effect of CLO concentration on corrosion data of mild steel in 2.0 M  $\text{H}_3\text{PO}_4$

Inhibitor	Concentration (g/L)	W ( $\text{mg cm}^{-2} \text{ h}^{-1}$ )	$\eta_w$ (%)	$\theta$
Blank	2.0	5.061	-	-
	0.25	1.556	69	0.69
CLO	0.5	1.371	73	0.73
	0.75	1.003	80	0.80
	1	0.834	83	0.83

### 3.4. Effect of the temperature

Effect of solution temperature (298–328 K) on corrosion inhibition efficiency of CLO in 1M HCl is listed in Table 4. It is observed that the value of  $\eta\%$  decreases on increasing solution temperature. The increase in solution temperature increases the kinetic energy of the CLO and therefore decreases the interaction between inhibitor and metal surface and thus decreases the inhibition efficiency. Further, increases in the solution temperature cause molecular decomposition resulting into decrease in the inhibition efficiency.

**Table 4.** The results of the temperature effect of carbon steel corrosion performed in 2.0 M  $\text{H}_3\text{PO}_4$  and with 1 g/L of CLO.

Medium	Temp. (K)	$C_R$ ( $\text{mg cm}^{-2} \text{h}^{-1}$ )	$\eta$ (%)	$\theta$
2.0 M $\text{H}_3\text{PO}_4$	298	5.061	-	-
	308	9.873	-	-
	318	16.411	-	-
	328	25.748	-	-
CLO	298	0.834	83	0.83
	308	1.905	80	0.80
	318	3.764	77	0.77
	328	7.333	71	0.71

The dependence of corrosion rate on temperature can be expressed by Arrhenius equation [4]:

$$C_R = A \exp\left(\frac{-E_a}{RT}\right) \quad (9)$$

where  $E_a$  represents apparent activation energy,  $R$  is the gas constant,  $A$  is the pre-exponential factor. The values of  $E_a$  were calculated by linear regression between  $\ln(C_R)$  and  $1/T$  (Figure 6). The value of  $E_a$  for inhibited solution is higher than that for uninhibited solution. The higher value of  $E_a$  in presence of almond oil indicates that more energy barrier is required for the corrosion reaction to occur [53].

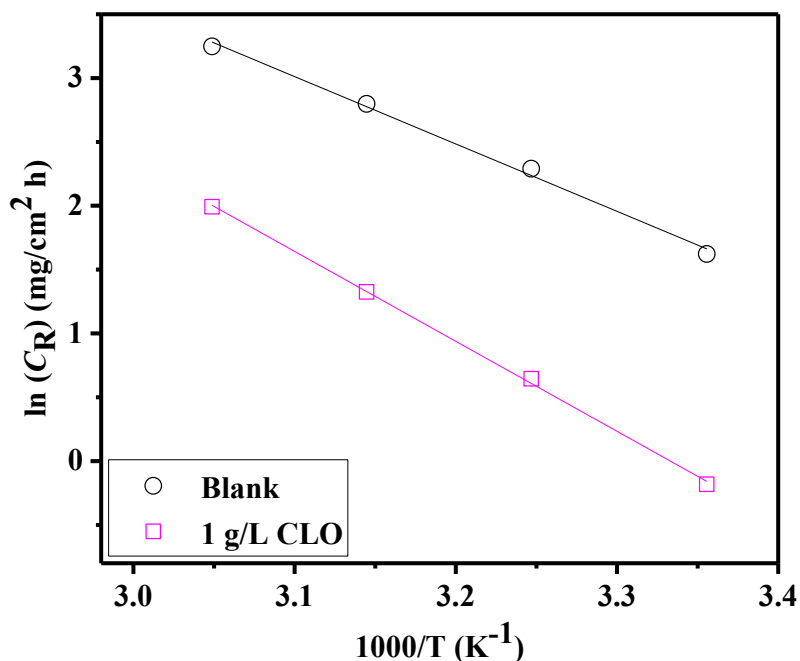


**Figure 6:** Arrhenius plots of  $\ln C_R$  vs.  $1/T$  for mild steel in 2.0 M  $\text{H}_3\text{PO}_4$  in the absence and the presence of CLO at optimum concentration.

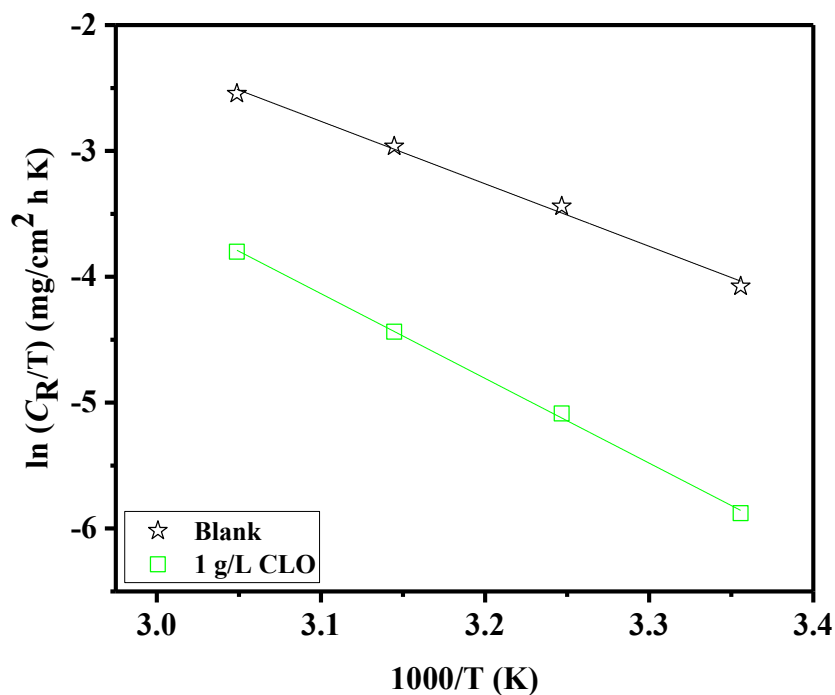


**Figure 7:** Relation between  $\ln(C_R/T)$  and  $1000/T$  at different temperatures.

Thermodynamics of mild steel corrosion in 2.0 M  $H_3PO_4$  are calculated using an alternative formula of the Arrhenius equation[4]:

$$C_R = \frac{RT}{Nh} \exp\left(\frac{\Delta S_a}{R}\right) \exp\left(-\frac{\Delta H_a}{RT}\right) \quad (10)$$

where  $h$  is Planck's constant,  $N$  is the Avogadro number,  $R$  is the universal gas constant,  $\Delta H_a$  is the enthalpy of activation and  $\Delta S_a$  is the entropy of activation. Figure 7 shows that the Arrhenius plots of  $\ln(C_R/T)$  versus  $1/T$  gave straight lines with slope  $(-\Delta H_a/R)$  and intercept  $(\ln R/Nh + \Delta S_a/R)$  from where  $\Delta H_a$  and  $\Delta S_a$  values were calculated.

The positive values of  $\Delta H_a$  in the presence and absence of inhibitor reflect the endothermic nature of steel dissolution. The higher values of  $\Delta S_a$  might be the result of the adsorption of almond oil molecules from the 2.0 M  $H_3PO_4$  solution, which could be regarded as a quasi-substitution process between oil molecules in the aqueous phase and water molecules on the mild steel surface[54].

**Table 5.** Activation parameters for the mild steel dissolution in 2.0 M  $H_3PO_4$  in the absence and the presence of 1 g/L of CLO.

Medium	$E_a$ (kJ mol <sup>-1</sup> )	$\Delta H_a$ (kJ mol <sup>-1</sup> )	$\Delta S_a$ (J mol <sup>-1</sup> K <sup>-1</sup> )
Blank	43.87	41.27	-92.48
CLO	58.58	55.97	58.28

### 3.5. Surface characterization

The scanning electron microscopy (SEM) images of mild steel surface in the absence and presence of optimum concentration of the investigated clove oil are shown in Figure 8. The SEM image of mild steel in the absence of CLO (Figure 8b) was highly corroded and damaged compared to polished steel (Figure 8a) which might be attributed to the free acid corrosion of the surface in the absence of CLO. However, in the presence of CLO at its optimum concentration (Figure 8c) the surface morphology remarkable smoothed owing to the formation of protective surface film.

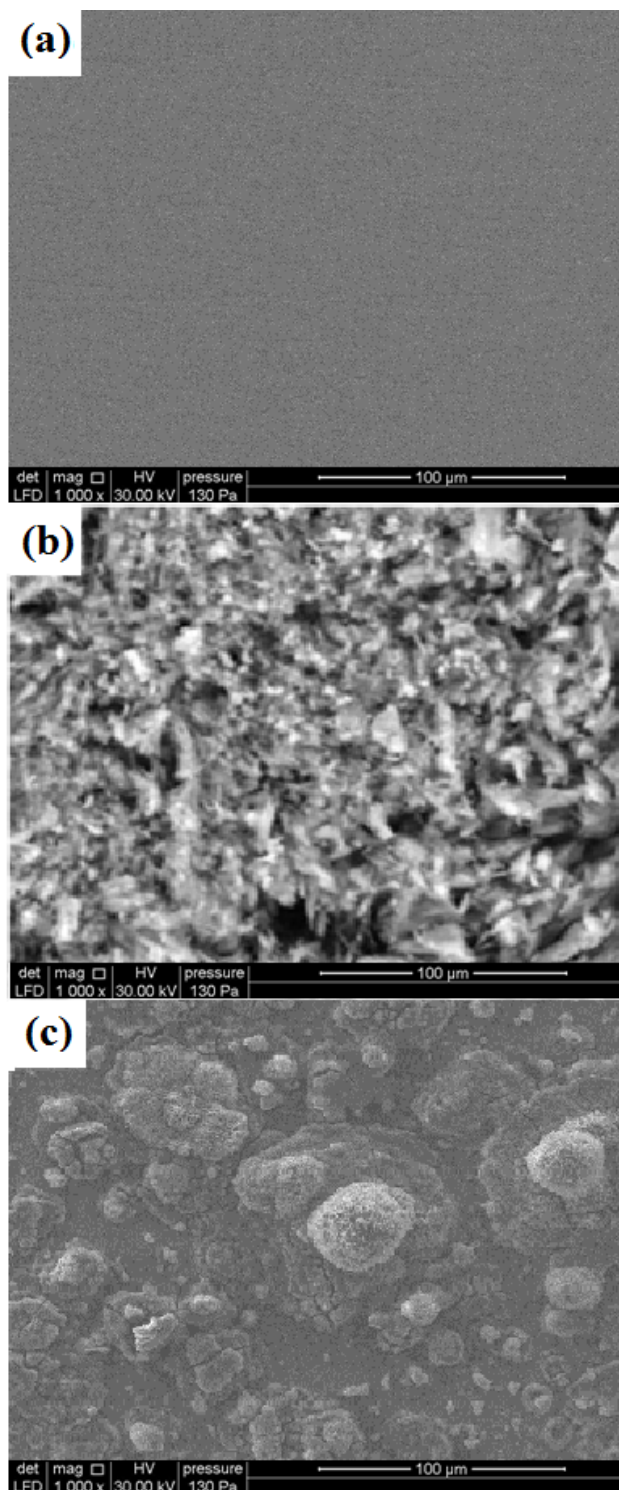


**Figure 8:** The SEM micrographs in polished steel (a) in absence (b) and presence (c) of CLO at 1 g/L.

### 3.5. DFT calculations

Quantum chemical methods enable the definition of a large number of molecular quantities characterizing the reactivity, shape, and binding properties of a complete molecule as well as of molecular fragments and substituents[32]. The geometry of the inhibitor as well as the nature of its frontier molecular orbitals, namely, the HOMO and LUMO is involved in the activity properties of the inhibitors[55]. Thus, in this study, quantum chemical calculations were performed to investigate the relationship between molecular structure of the Eugenol which is the main constituent of the clove oil and their inhibition effect. The optimized molecular structure and the frontier molecule orbital density distribution of the studied molecule are shown in Figure 9, and the calculated quantum chemical indices  $E_{\text{HOMO}}$ ,  $E_{\text{LUMO}}$ ,  $\Delta E$  are given in Table 7. From this figure, it can be seen that the electron density is saturated all around eugenol molecule which should facilitate flat-lying adsorption orientations.

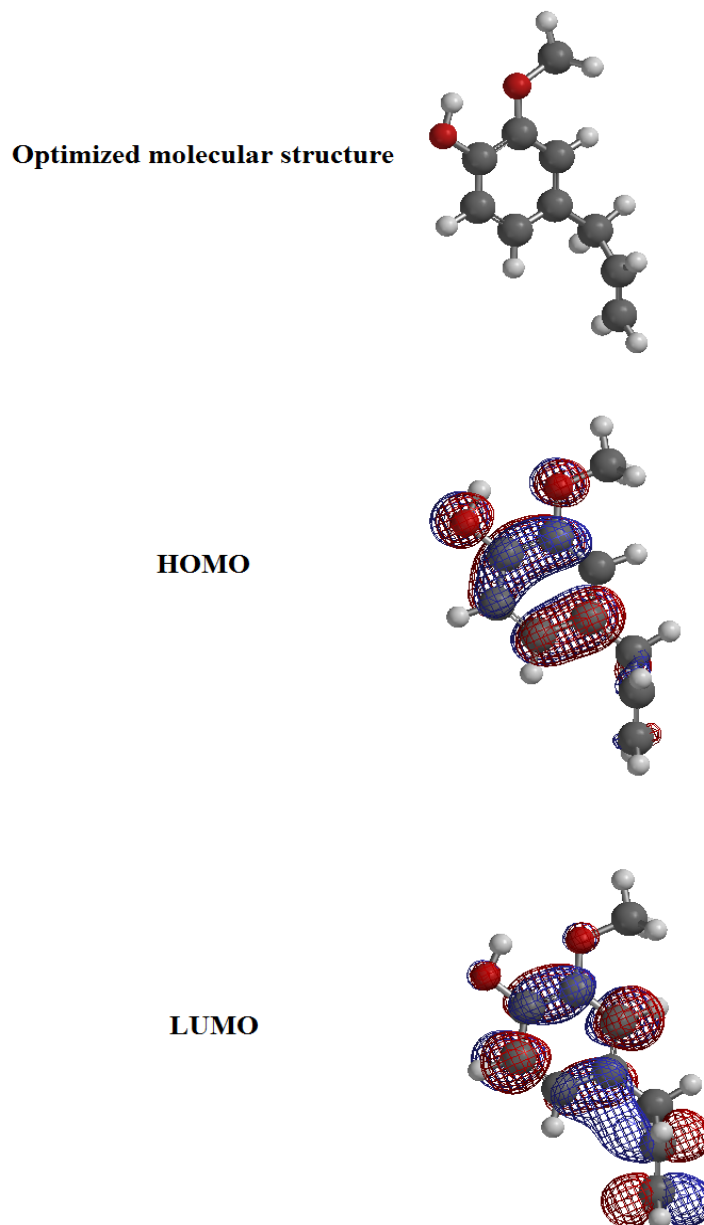


**Figure 9:** Localization of HOMO and LUMO of Eugenol calculated by DFT.

A high  $E_{\text{HOMO}}$  value expresses intrinsic electron donating tendency to an appropriate acceptor, i.e., any molecule with lower HOMO energy and empty molecular orbital while,  $E_{\text{LUMO}}$ , the energy of the lowest unoccupied molecular orbital signifies the electron receiving tendency of a molecule [32,55]. The difference between the  $E_{\text{HOMO}}$  and the  $E_{\text{LUMO}}$  energies ( $\Delta E$ ) gives an indication of the chemical reactivity of a molecule [55]. According to Table 6, the high value of  $E_{\text{HOMO}}$ , lower value of  $E_{\text{LUMO}}$  and a small  $\Delta E$  indicates a higher interaction between the metal surface and inhibitor molecules [56,57]. The number of electron transfer ( $\Delta N$ ) was calculated using the following equation [58]:

$$\Delta N = \frac{\phi - \chi_{\text{inh}}}{2(\eta_{\text{Fe}} + \eta_{\text{inh}})}$$

Where  $\phi$  and  $\chi_{\text{inh}}$  denote the work function and absolute electronegativity of the inhibitor molecule, respectively;  $\eta_{\text{Fe}}$  and  $\eta_{\text{inh}}$  are the absolute hardness of mild steel and the inhibitor molecule, respectively. The above quantum chemical parameters are related to electron affinity (EA) and ionization potential (IP)[59].

$$\chi = \frac{IP + EA}{2} \quad (11)$$

$$\eta = \frac{IP - EA}{2}$$

Where  $IP = -E_{HOMO}$  and  $EA = -E_{LUMO}$ .

$\chi$  and  $\eta$  are calculated using the values of IP and EA. The theoretical values of  $\phi$  and  $\eta$  of Fe are 4.82 eV [60,61] and 0 eV, respectively. According to Lukovits et al. [62], if the value of  $\Delta N$  is less than 3.6, the efficiency of inhibition increases with increasing electron-donating ability of the inhibitor to the metal surface.

**Table 6.** Quantum theoretical parameters for Eugenol calculated using DFT.

$E_{HOMO}$ (eV)	$E_{LUMO}$ (eV)	$\Delta E$ (eV)	$\Delta N$
-5.4	0.2	5.6	0.396

### 3.6. MD simulations

The adsorption of the Eugenol molecule on the metal surface was analyzed at a molecular level by molecular dynamics simulations to sample many different low energy configurations and identify the low energy minima[55]. Figure 10 shows representative snapshots of the crosssection of the lowest energy adsorption configurations for the single molecule on the Fe (110) surface from our simulations.

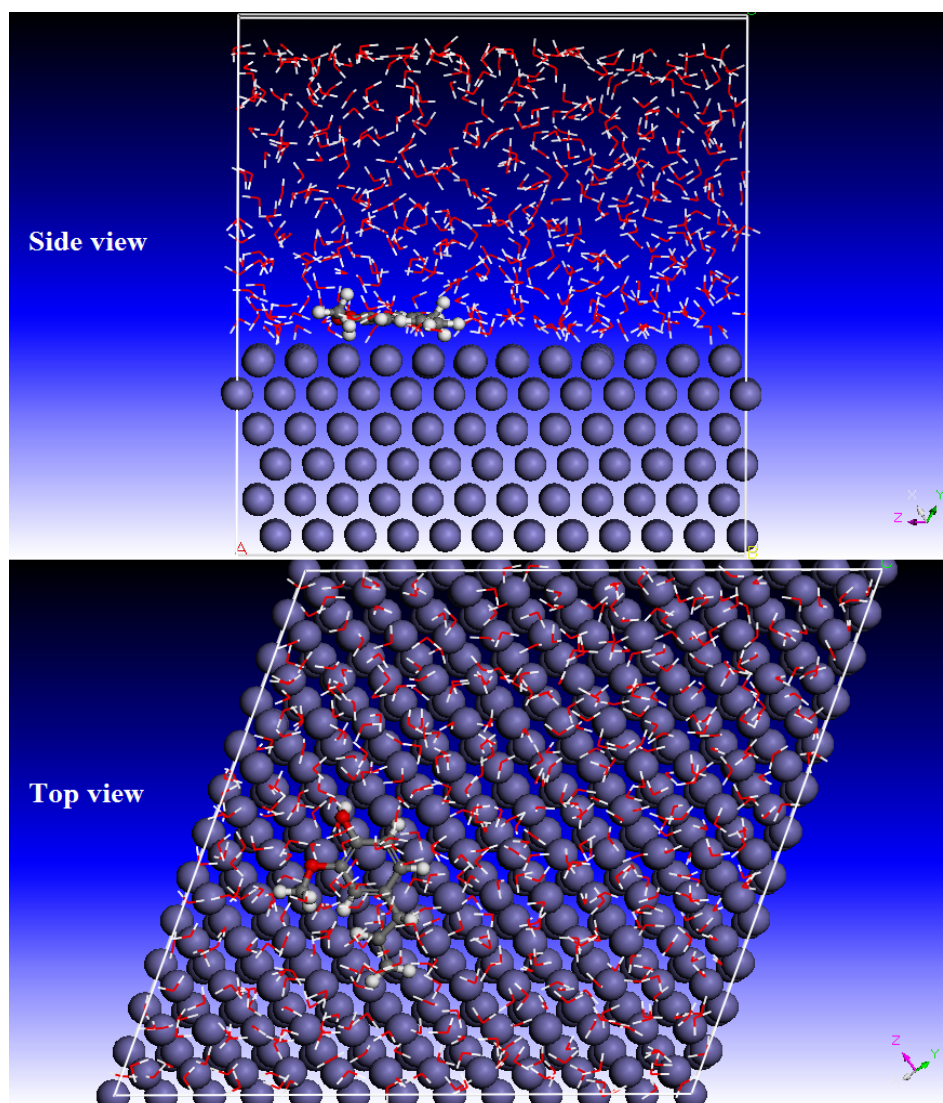


**Figure 10:** Representative snapshots of Eugenol on Fe (1 1 0) surface.

The molecules can be seen to maintain a flat-lying adsorption orientation on the Fe surface, in order to maximize contact and enhance the degree of surface coverage. This parallel adsorption orientation also facilitates interaction of  $\pi$ -electrons of the benzene ring and the heteroatoms with the metal surface. The binding energy of the adsorption system is 303.44 kJ/mol. The magnitude of binding energy is indicative of stability of adsorptive system, and higher positive value of binding energy indicates inhibitor adsorb on the iron surface easier [55,63,64].

## Conclusion

Results show that CLO acts as good corrosion inhibitor for mild steel in 2.0 M H<sub>3</sub>PO<sub>4</sub> and their inhibition efficiency increases with increasing concentration. The optimum concentration of 1g/L can decrease the corrosion of material with the efficiency of 87%. The adsorption of clove oil inhibitor obeys the Langmuir adsorption isotherm. The polarization study revealed that the CLO acts as mixed type inhibitor. The presence of the CLO increases the polarization resistance values and therefore inhibits mild steel corrosion. The SEM well support the weight loss and electrochemical finding. Data obtained from quantum chemical calculations using DFT and MD simulations were correlated to the inhibitive effect of Eugenol. Both experimental and theoretical calculations are in excellent agreement.

## References

1. B. El Makrini, H. Lgaz, K. Toumiat, R. Salghi, S. Jodeh, G. Hanbali, M. Belkhaouda, M. Zougagh, *Res. J. Pharm. Biol. Chem. Sci.* 7 (2016) 2277–2285.
2. M. Larouj, H. Lgaz, H. Serrar, H. Zarrok, H. Bourazmi, A. Zarrouk, A. Elmidaoui, A. Guenbour, S. Boukhris, H. Oudda, *J. Mater. Environ. Sci.* 6 (2015) 3251–3267.
3. L. Adardour, H. Lgaz, R. Salghi, M. Larouj, S. Jodeh, M. Zougagh, O. Hamed, H. Oudda, *Pharm. Lett.* 8 (2016) 212–224.
4. H. Lgaz, M. Saadouni, R. Salghi, S. Jodeh, Y. Ramli, A. Souizi, H. Oudda, *Pharm. Lett.* 8 (2016) 167–179.
5. H. Lgaz, A. Anejjar, R. Salghi, S. Jodeh, M. Zougagh, I. Warad, M. Larouj, P. Sims, *Int. J. Corros. Scale Inhib.* 5 (2016) 209–231.
6. T. Laabaissi, H. Lgaz, H. Oudda, F. Benhiba, H. Zarrok, A. Zarrouk, A. El Midaoui, B. Lakhrissi, R. Tourir, *J. Mater. Environ. Sci.* 8 (2017) 1054–1067.
7. A. Bousskri, A. Anejjar, R. Salghi, S. Jodeh, R. Touzani, L. Bazzi, H. Lgaz, *J. Mater. Environ. Sci.* 7 (2016) 4269–4289.
8. M. Saadouni, M. Larouj, R. Salghi, H. Lgaz, S. Jodeh, M. Zougagh, A. Souizi, *Pharm. Lett.* 8 (2016) 65–76.
9. H. Lgaz, S. Rachid, M. Larouj, M. Elfaydy, S. Jodeh, H. About, B. Lakhrissi, K. Toumiat, H. Oudda, *Mor. J. Chem.* 4 (2016) 592–612.
10. L. Adardour, H. Lgaz, R. Salghi, M. Larouj, S. Jodeh, M. Zougagh, O. Hamed, M. Taleb, *Pharm. Lett.* 8 (2016) 173–185.
11. L. Adardour, H. Lgaz, R. Salghi, M. Larouj, S. Jodeh, M. Zougagh, I. Warad, H. Oudda, *Pharm. Lett.* 8 (2016) 126–137.
12. H. Lgaz, R. Salghi, S. Jodeh, *Int. J. Corros. Scale Inhib.* 5 (2016) 347–359.
13. B. El Makrini, K. Toumiat, H. Lgaz, R. Salghi, S. Jodeh, G. Hanbali, M. Belkhaouda, M. Zougagh, *Res. J. Pharm. Biol. Chem. Sci.* 7 (2016) 2286–2294.
14. L. Adardour, M. Larouj, H. Lgaz, M. Belkhaouda, R. Salghi, S. Jodeh, A. Salman, H. Oudda, M. Taleb, *Pharma Chem.* 8 (2016) 152–160.
15. S. Skal, Y. Kerroum, A. Guenbour, A. Bellaouchou, H. Tabyaoui, H. Idrissi, A. Zarrouk, J. García-Antón, *J. Mater. Environ. Sci.* 8 (2017) 3234–3246.
16. G. Gunasekaran, L.R. Chauhan, *Electrochimica Acta.* 49 (2004) 4387–4395.
17. B. El Makrini, H. Lgaz, M. Larouj, R. Salghi, A. Rasem Hasan, M. Belkhaouda, S. Jodeh, M. Zougagh, H. Oudda, *Pharma Chem.* 8 (2016) 256–268.
18. O. Krim, O. Krim, M. Messali, B. Hammouti, A. Elidrissi, K. Khaled, R. Salghi, H. Lgaz, *Port. Electrochimica Acta.* 34 (2016) 213–229.
19. H. Lgaz, Y. ELaoufir, Y. Ramli, M. Larouj, H. Zarrok, R. Salghi, A. Zarrouk, A. Elmidaoui, A. Guenbour, E.M. Essassi, H. Oudda, *Pharma Chem.* 7 (2015) 36–45.
20. Y. El Aoufir, H. Lgaz, H. Bourazmi, Y. Kerroum, Y. Ramli, A. Guenbour, R. Salghi, F. El-Hajjaji, B. Hammouti, H. Oudda, *J. Mater. Environ. Sci.* 7 (2016) 4330–4347.
21. H. Lgaz, O. Benali, R. Salghi, S. Jodeh, M. Larouj, O. Hamed, M. Messali, S. Samhan, M. Zougagh, H. Oudda, *Pharma Chem.* 8 (2016) 172–190.
22. Y. El Aoufir, H. Lgaz, K. Toumiat, R. Salghi, S. Jodeh, M. Zougagh, A. Guenbour, H. Oudda, *Res. J. Pharm. Biol. Chem. Sci.* 7 (2016) 1219–1227.
23. A.Y. El-Etre, A.I. Ali, *Chin. J. Chem. Eng.* 25 (2017) 373–380.
24. M.S. Uwineza, M. Essahli, A. Lamiri, *Port. Electrochimica Acta.* 34 (2016) 53–62.
25. M. Benabdellah, M. Benkaddour, B. Hammouti, M. Bendahhou, A. Aouniti, *Appl. Surf. Sci.* 252 (2006) 6212–6217.
26. K. Orubite, N. Oforka, *Mater. Lett.* 58 (2004) 1768–1772.

27. F. Fang, K. Candy, E. Melloul, C. Bernigaud, L. Chai, C. Darmon, R. Durand, F. Botterel, O. Chosidow, A. Izri, W. Huang, J. Guillot, *Parasit. Vectors.* 9 (2016) 594.
28. A. Saxena, A. Sharma, D. Saxena, P. Jain, *J. Chem.* 9 (2012) 2044–2051.
29. S. Tazi, I. Raissouni, F. Chaoukat, D. Bouchta, A. Dahdouh, R. Elkhamlichi, H. Douhri, *J. Mater. Environ. Sci.* 7 (2016) 1642–1652.
30. M. Abdallah, S.O.A. Karanee, A.A.A. Fattah, *Chem. Eng. Commun.* 196 (2009) 1406–1416.
31. A. Fouda, G. Elewady, K. Shalabi, H.A. El-Aziz, *RSC Adv.* 5 (2015) 36957–36968.
32. A. Liu, X. Ren, J. Zhang, C. Wang, P. Yang, J. Zhang, M. An, D. Higgins, Q. Li, G. Wu, *RSC Adv.* 4 (2014) 40606–40616.
33. S. Issaadi, T. Douadi, S. Chafaa, *Appl. Surf. Sci.* 316 (2014) 582–589.
34. Wavefunction Inc., Spartan '14 version 1.1.0, 18401 Von Karman Ave., Suite 370, Irvine CA 92612, 2013.
35. Materials Studio, Revision 6.0, Accelrys Inc., San Diego, USA, 2013.
36. Z. Salarvand, M. Amirnasr, M. Talebian, K. Raeissi, S. Meghdadi, *Corros. Sci.* 114 (2017) 133–145.
37. A.Y. Musa, R.T. Jalgham, A.B. Mohamad, *Corros. Sci.* 56 (2012) 176–183.
38. S.K. Saha, P. Ghosh, A. Hens, N.C. Murmu, P. Banerjee, *Phys. E Low-Dimens. Syst. Nanostructures.* 66 (2015) 332–341.
39. R. Solmaz, G. Kardaş, M. Culha, B. Yazıcı, M. Erbil, *Electrochimica Acta.* 53 (2008) 5941–5952.
40. M. El Achouri, S. Kertit, H. Gouttaya, B. Nciri, Y. Bensouda, L. Perez, M. Infante, K. Elkacemi, *Prog. Org. Coat.* 43 (2001) 267–273.
41. K. Toumiat, Y. El Aoufir, H. Lgaz, R. Salghi, S. Jodeh, M. Zougagh, H. Oudda, *Res. J. Pharm. Biol. Chem. Sci.* 7 (2016) 1210–1218.
42. C. Verma, M.A. Quraishi, A. Singh, *J. Mol. Liq.* 212 (2015) 804–812.
43. H. Lgaz, R. Salghi, S. Jodeh, B. Hammouti, *J. Mol. Liq.* 225 (2017) 271–280.
44. M.A. Amin, M. Ahmed, H. Arida, T. Arslan, M. Saracoglu, F. Kandemirli, *Corros. Sci.* 53 (2011) 540–548.
45. M.A. Amin, S.A. El-Rehim, E. El-Sherbini, R.S. Bayoumi, *Int J Electrochem Sci.* 3 (2008) 199–215.
46. K.R. Ansari, M.A. Quraishi, A. Singh, *J. Ind. Eng. Chem.* 25 (2015) 89–98.
47. K. Khaled, *Electrochimica Acta.* 53 (2008) 3484–3492.
48. A. Bousskri, R. Salghi, A. Anejjar, S. Jodeh, M.A. Quraishi, M. Larouj, H. Lgaz, M. Messali, S. Samhan, M. Zougagh, *Pharma Chem.* 8 (2016) 67–83.
49. N.K. Gupta, M.A. Quraishi, C. Verma, Mukherjee, A. K., *RSC Advances*, 6(104), 102076–102087.
50. C. Verma, M.A. Quraishi, A. Singh, *J. Mol. Liq.* 212 (2015) 804–812.
51. H. Lgaz, O. Benali, R. Salghi, S. Jodeh, M. Larouj, O. Hamed, M. Messali, S. Samhan, M. Zougagh, H. Oudda, *Pharma Chem.* (2016) 172–190.
52. E. Chaieb, A. Bouyanzer, B. Hammouti, M. Benkaddour, *Applied Surface Science*, 246 (2005) 199–206
53. K. Ansari, D.K. Yadav, E.E. Ebenso, M. Quraishi, *Int J Electrochem Sci.* 7 (2012) 4780–4799.
54. I. Obot, N. Obi-Egbedi, *Curr. Appl. Phys.* 11 (2011) 382–392.
55. F.E. Awe, S.O. Idris, M. Abdulwahab, E.E. Oguzie, *Cogent Chem.* 1 (2015) 1112676.
56. I. Danaee, O. Ghasemi, G.R. Rashed, M. Rashvand Avei, M.H. Maddahy, *J. Mol. Struct.* 1035 (2013) 247–259
57. K. Ramya, R. Mohan, K.K. Anupama, A. Joseph, *Mater. Chem. Phys.* 149–150 (2015) 632–647.
58. X. Li, S. Deng, X. Xie, *J. Taiwan Inst. Chem. Eng.* 45 (2014) 1865–1875.
59. X. Li, S. Deng, X. Xie, *Corros. Sci.* 81 (2014) 162–175.
60. Z. Cao, Y. Tang, H. Cang, J. Xu, G. Lu, W. Jing, *Corros. Sci.* 83 (2014) 292–298.
61. A. Kokalj, *Chem. Phys.* 393 (2012) 1–12.
62. I. Lukovits, E. Kalman, F. Zucchi, *Corrosion.* 57 (2001) 3–8.
63. Y. Yan, X. Wang, Y. Zhang, P. Wang, J. Zhang, *Mol. Simul.* 39 (2013) 1034–1041.
64. D. Zhang, Y. Tang, S. Qi, D. Dong, H. Cang, G. Lu, *Corros. Sci.* 102 (2016) 517–522.

(2018) ; <http://www.jmaterenvironsci.com>